Intrinsic vulnerabilities to mechanical failure in nanoscale films

Pooja Shah [a], Thomas M. Truskett [a,b,*]

[a]*Department of Chemical Engineering and*

[b]*Institute for Theoretical Chemistry, The University of Texas at Austin, Austin,*

Texas 78712, USA

Abstract

We use molecular simulations to explore how sample dimensions and interfacial properties impact some generic aspects of the mechanical and structural behavior of nanoconfined materials. Specifically, we calculate the strain-dependent properties of minimum-energy thin-film particle configurations (i.e., inherent structures) confined between attractive, parallel substrates. We examine how the relationship between the transverse strain and the stress tensor (the equation of state of the energy landscape) depends on the properties of the film and substrate. We find that both film thickness and film-substrate attractions influence not only the mechanical properties of thin films, but also the shape and location of the "weak spots" where voids preferentially form in a film as it is strained beyond its point of maximum tensile stress. The sensitivity of weak spots to film properties suggests that nanoscale materials may be intrinsically vulnerabile to specific mechanisms of mechanical failure.

Key words: Nanoscale films; Mechanical failure; Potential energy landscape; Molecular simulations.

1   Introduction

Materials confined to very small spatial dimensions behave differently than in the bulk. In addition to showing quantum confinement effects, they also display thermodynamic, kinetic, and mechanical limits of stability that depend on sample size, shape, and the characteristics of their interfaces. Specific examples of property modifications include surface-induced phase transitions, shifts of the bulk glass transition, and interface-mediated modes of mechanical failure (Gelb et. al, 1999; Forrest and Dalnoki-Veress, 2001; Hutchinson and Suo, 1992). Unfortunately, because molecular-scale processes in highly inhomogeneous environments are difficult to resolve experimentally, a mechanistic picture for precisely how nanoconfinement impacts stability has been slow to develop. This presents a practical barrier to the design of technological applications, in particular those relying on solid-state nanostructures to exhibit mechanical integrity over a broad range of conditions.

In this Article, we study an elementary model system that sheds new light on how sample dimensions and interfacial properties can influence the mechanical behavior of nanoconfined materials. Specifically, we use molecular simulations to calculate the strain-dependent properties of mechanically-stable films of particles confined between attractive, parallel substrates. Although analogous studies have been carried out for models of isotropic materials, this is, to

* Corresponding author. Tel.: +1-512-471-6308; fax: +1-512-471-7060
  Email address: `truskett@che.utexas.edu` (Thomas M. Truskett).

our knowledge, the first systematic investigation of the relationship between the transverse strain and the pressure tensor of the inherent structures (minimum potential energy configurations) of highly inhomogeneous films. Our main finding is that both sample dimensions and substrate attractions substantially influence not only the mechanical properties of thin films, but also the morphology and location of "weak spots" where voids preferentially form in a film as it is strained beyond its point of maximum tensile stress. Although the precise role that these weak spots play in dynamic deformation processes is presently unknown, they appear intimately linked to material failure by quasistatic tensile deformation. Moreover, the sensitivity of weak spots to film properties suggests that nanoscale materials may be intrinsically vulnerabile to specific mechanisms of mechanical failure.

Since plastic deformation and failure are inherently dynamic events, and since the molecular-scale rearrangements that accompany them in amorphous materials are still poorly understood, molecular dynamics (MD) simulations would appear to represent an ideal theoretical tool for their investigation. In fact, MD simulation studies over the past decade have been instrumental in gaining insights into deformation processes in polymeric and small-molecule materials (Falk and Langer, 1998; Gersappe and Robbins, 1999; Rottler and Robbins, 2001, 2003; Stevens, 2001; Gersappe, 2002; Capaldi et al., 2002; Varnik et al., 2004; Van Workum and de Pablo, 2003; Yoshimoto et al., 2004). These insights have facilitated the interpretation of experiments and have aided in the introduction of simple theories for viscoplastic flow (Falk and Langer, 1998). On the other hand, despite recent advancements in algorithms for long-time dynamics, MD simulations are still limited to accessing relatively short time and length scales. Thus, it is currently computationally prohibitive to use MD

to exhaustively explore the effects that sample dimensions and interfacial conditions have on the mechanisms of mechanical failure, even for simple model systems. The development of alternative methods for probing the molecular-scale origins of failure in glasses is still essential.

One complimentary approach is to calculate how the properties of a material's mechanically-stable inherent structures depend on the state of strain. This strategy has typically been implemented in one of two ways to investigate deformation, tensile strength, and failure of amorphous solids. The first method (Mott et al., 1993; Hutnik et al., 1993; Malandro and Lacks, 1997, 1998, 1999; Lund and Schuh, 2003a,b; Maloney and Lemaître, 2004a,b) calls for subjecting an ensemble of inherent structures, created at a prescribed state of strain or stress, to an athermal quasistatic deformation process consisting of alternating steps of small affine deformation followed by potential energy minimization. Malandro and Lacks (1997, 1998, 1999) have used this protocol to investigate the connection between strain-induced plastic rearrangements in amorphous materials and the annihilation of minima on the material's potential energy landscape. A similar implementation has also been used by Maloney and Lemaître (2004a,b) to study the energy fluctuations associated with amorphous plasticity and the behavior of elastic constants near the onset of material failure.

Alternatively, one can generate collections of inherent structures at each macroscopic strain state of interest by mapping equilibrium particle configurations from high-temperature simulations to their local potential energy minima (Stillinger and Weber, 1982). This procedure, which we adopt here, has been primarily employed by Debenedetti, Stillinger, and collaborators (Sastry et al., 1997; Roberts et al., 1999; Utz et al., 2001; Shen et al., 2002) to determine

how the inherent structure pressure of 'bulk' glass-formers depends on density, a relationship that has been termed the *equation of state of an energy landscape* (EOSEL) (Debenedetti et al., 1999). Several trends have emerged from simulated EOSELs that give insights into the mechanical properties of amorphous solids. For example, inherent structures formed with densities higher than the material's Sastry density ρ_S (shown in Fig 1a) are structurally homogeneous, whereas "weak spots" (Sastry et al., 1997) contained in lower-density equilibrium configurations develop into fissures or voids upon energy minimization. Thus, ρ_S is a material property that represents the minimum density for which mechanically-stable solid structures can remain structurally homogeneous and void free. Moreover, the corresponding isotropic tension $-p_{IS}(\rho_S)$ is the maximum amount that an inherent structure of that material can sustain prior to rupture. Note that ρ_S obtained from the EOSEL is conceptually similar to the density of maximum isotropic tensile stress obtained from a quasistatic expansion process, and, in fact, recent simulations (Shen et al., 2002) show quantitative agreement between these two densities for a number of model materials.

2 Probing Vulnerabilities to Failure in Nanoscale Films

The EOSELs of ultrathin films have been recently predicted by an approximate mean-field theory (Mittal et al., 2004; Truskett and Ganesan, 2003), but, to our knowledge, they have never been determined via molecular simulation. One naturally expects far richer behavior in thin films than in bulk materials because interfacial interactions render them anisotropic and statistically inhomogeneous. One consequence, illustrated in Fig. 1b, is the emergence of two

5

distinct versions of the curve shown in Fig. 1a, representing the density dependencies of the transverse $(p_{IS}^{\parallel})$ and normal $(p_{IS}^{\perp})$ components of the inherent structure pressure tensor. This additional dimension of the EOSEL prompts several new questions pertaining to the film's intrinsic vulnerabilities to mechanical failure. For example, how do film thickness and substrate attractions affect the directionality of mechanical failure (i.e., which component of the stress tensor will exhibit a maximum at a smaller value of strain)? Moreover, is structural failure (i.e., void formation) initiated at the strain of maximal stress as it is in bulk materials (Sastry et al., 1997; Debenedetti et al., 1999)? If so, do film thickness and substrate attractions strongly influence the location and the morphology of the corresponding voids?

To investigate these issues, we calculated the EOSEL of model films comprising $N = 864$ Lennard-Jones (LJ) particles (truncated and shifted at $r = 2.5$ (Sastry et al., 1997)) confined between parallel substrates that interact with them through an effective 9-3 LJ potential,

$$v_{fw}(z) = \frac{2\pi}{3}\rho_w \sigma_w^3 \epsilon_w \left[\frac{2}{15} \left(\frac{\sigma_w}{z} \right)^9 - \left(\frac{\sigma_w}{z} \right)^3 \right] \tag{1}$$

Here, z is the distance between substrate and particle center, $\rho_w \sigma_w^3 = 0.988$, and $\sigma_w = 1.0962$ (Ebner and Saam, 1977). All quantities reported in this work are implicity nondimensionalized by the standard combinations of length and energy scales provided by the effective diameter σ and the well-depth ϵ of the LJ film particles, respectively. Periodic boundary conditions were applied in the x and y directions to simulate a system of infinite transverse extent. Additional simulations (not shown here) using $N = 1024$ and $N = 2048$ particles were also carried out to verify that the results were insensitive to N.

The effects of film thickness and strength of the film-substrate attractions were examined by simulating nine films characterized by the permutations of the following substrate separations $L \in \{5, 7.5, 10\}$ and film-substrate well depths $\epsilon_w \in \{0.2\epsilon_{fw}, \epsilon_{fw}, 5\epsilon_{fw}\}$, where $\epsilon_{fw} = 1.2771$ (Ebner and Saam, 1977). The inherent structures required for the EOSEL analysis were obtained by mapping high-temperature ($T = 2.5$) equilibrium configurations from a series of fluid film densities in the range $\rho = 0.2 - 1.0$ to their local potential energy minima using LBFGS (Liu and Nocedal, 1989), a limited-memory quasi-Newton multidimensional optimization routine. The equilibrium configurations were generated by Monte Carlo simulations in the canonical ensemble. For every film type and strain state, 100 equilibrium configurations (separated by 500 Monte Carlo cycles) were selected for minimization. The components of the inherent structure pressure tensor were calculated both by the global virial equation (Born and Huang, 1954) and by spatially averaging the local Irving and Kirkwood (1950) expressions. The two approaches produced indistinguishable results.

For the structural analysis of the inherent structure configurations, *void space* was defined to be the volume of film comprising all points that lie both a distance $d > 1$ from any particle center and $d > (\sigma_w + 1)/2$ from either substrate. The void probability is then simply the fractional film volume available for insertion of an additional particle center without creating "overlap" with an existing particle or substrate. For each strain state, the average void probability was calculated by performing 10^6 trial insertions of hard-core test particles of unit diameter. These data were binned according to normal position z to determine the film's inhomogeneous void probability profiles. The methods described above for both generating and analyzing our thin-film struc-

tures follow directly from established techniques for studying bulk materials, and the interested reader can find more information in recent review articles by Debenedetti et al. (1999, 2001).

As a final point, we discuss the main rationale for choosing the LJ model for our initial investigation. First, it is a microscopic model that shows qualitatively realistic mechanical and structural behavior (Sastry et al., 1997), but it also is simple enough to allow a systematic investigation of the effects of interfaces and confinement on its properties. Moreover, since the bulk LJ system is already well characterized (Sastry et al., 1997; Debenedetti et al., 1999), any confinement-induced deviations should be relatively straightforward to recognize and interpret. Finally, a knowledge of these deviations will provide a useful basis for understanding future simulations on materials with richer molecular attributes.

3   Results and Discussion

In this section, we study how the specific properties of our model LJ films impact their vulnerability to various modes of mechanical failure. To accomplish this, we investigate how sample dimensions and film-substrate attractions affect the strain dependencies of the stress tensor and the void-space morphology of thin-film inherent structures. The locations and shapes of the voids or 'weak spots' that appear in the films when they are strained beyond their maximal stress states provide markers for the corresponding mechanisms of failure. We discuss how these mechanisms arise from structural inhomogeneities in the film and the properties of the film-substrate interfaces.

Fig. 2a shows the simulated EOSEL of an ultrathin film ($L = 5$) confined between 'weakly attractive' substrates ($\epsilon_w = 0.2\epsilon_{fw}$). Note that $p_{IS}^{\perp}$ exhibits a minimum at a higher value of density than does $p_{IS}^{\parallel}$, or, equivalently, the maximum normal stress corresponds to a smaller strain than does the maximum transverse stress. Thus, from a mechanical perspective, the inherent structure film can be considered more vulnerable to failure in the normal direction when subjected to plane strain. Fig. 2a also illustrates that, as is observed in the bulk (Sastry et al., 1997; Debenedetti et al., 1999), the probability of finding voids in the film becomes non-neglible for densities below the maximal stress state. This connection between mechanical and structural failure is examined more closely in the void probability profiles and film images of Fig. 2b and 2c, respectively. As can be seen, the main structural effect of transverse strain is the formation of planar voids where the film detaches from one of the substrates, indicating an *adhesive* mechanism for mechanical failure.

One natural question to ask is, do substrate attractions noticeably affect the film's mechanical and structural vulnerabilities to failure? Fig. 3 shows the EOSEL for an ultrathin film ($L = 5$) with 'strongly attractive' substrates ($\epsilon_w = 5\epsilon_{fw}$). Comparison of Fig. 2a and 3a shows that, at least for ultrathin films ($L = 5$), there seem to be some features of the EOSEL that are independent of the strength of the substrate attractions. For example, the film confined between strongly attractive substrates also shows mechanical vulnerability to failure in the normal direction, with $p_{IS}^{\perp}$ exhibiting its minimum at a higher value of density than $p_{IS}^{\parallel}$. Moreover, Fig. 3a shows a similar correspondence between the attainment of maximal stress and the initial appearance of voids in the film. However, the key difference can be found in the location of the 'weak spots' where strain-induced voids appear. As is evidenced by the void

profiles and film images of Fig. 3b and 3c, the strongly attractive substrates promote a *cohesive* rather than adhesive failure mechanism, indicated by the formation of planar voids between the molecular layers in the center of the film. This mode of failure results in films with much larger tensile strength and toughness than films that fail adhesively.

The main physical result from Fig. 2 and 3 is that strain-induced local stresses in highly inhomogeneous films, dictated by the relative strengths of the interparticle and film-substrate attractions, introduce specific types of vulnerabilities to failure (e.g., adhesive or cohesive failure). These vulnerabilities have important implications for the material properties of the films. Interestingly, there is also preliminary evidence to suggest that such energetic vulnerabilities may strongly influence the actual mechanisms of dynamic failure events. In particular, recent MD simulations of polymeric thin films confined between solid substrates (Gersappe and Robbins, 1999) have found that the transition from adhesive to cohesive mechanisms of failure is essentially independent of temperature and, moreover, that it is primarily controlled by the strength of substrate attractions. The fact that both dynamic and EOSEL-type simulation studies provide a similar physical picture is intriguing. However, more systematic investigations of the energetic and entropic contributions to dynamic failure events in model systems will be necessary to assess the generality of these observations.

To explore the impact of thickness L on the mechanical and structural properties of nanoscale films, we consider two additional cases. The first, shown in Fig. 4a, is the EOSEL of a thicker film ($L = 10$) confined between strongly attractive substrates ($\epsilon_w = 5\epsilon_{fw}$). Note that considerable asymmetry between $p_{IS}^{\perp}$ and $p_{IS}^{\parallel}$ is still apparent in thicker films, with the former component at-

taining a larger magnitude of maximum tensile stress at a slightly smaller value of plane strain. This behavior reflects the fact that film particles are strongly attracted to the substrates, making it favorable for the film to accomodate plane strain by tearing itself apart internally. However, the proximity of the strains of maximal normal and tensile stress in Fig. 4a (as compared to Fig. 3a) suggests that one can expect differences between the structural mechanisms of failure for thicker versus ultrathin films.

To interrogate the microscopic origins of these differences, we look to the void space analysis. As can be seen by comparing Fig. 4b and 4c to Fig. 3b and 3c, cohesive failure does show qualitatively different structural consequences in ultrathin and thicker films. While ultrathin films fail by forming planar voids between molecular layers parallel to the substrates, thicker films generally fail by forming voids that are 'local' and more isotropic (more balanced in the transverse and normal directions), not so different from the "bubble-like" voids that form from weak spots in bulk materials (Sastry et al., 1997; Shen et al., 2002). Note that this local cohesive failure mechanism produces a film with a much smaller tensile strength than the ultrathin film of Fig. 3.

The second thicker-film case ($L = 10$) that we examine is the one confined between neutral substrates ($\epsilon_w = \epsilon_{fw}$). What type of failure mechanism is expected to prevail for this film? Fig. 4 shows that in thicker films, like in bulk materials, there is a strong tendency to cavitate upon expansion due local cohesive stresses. However, since the substrates are not nearly as attractive in the neutral wall film, it is not clear at the outset whether cavitation will be controlled by the cohesive stresses in the normal direction (as in Fig. 4) or in the transverse direction.

The EOSEL shown in Fig. 5a displays only slight asymmetry in the normal and transverse pressure tensor components, indicating that the two aforementioned mechanisms for failure (normal cohesive and transverse cohesive) are in close competition. In contrast to the results of Fig. 4a, $p_{IS}^{\parallel}$ in the neutral wall film exhibits its minimum at a density slightly larger than does $p_{IS}^{\perp}$. This suggests that there is a preference for the transverse cohesive mechanism for failure.

To see the structural consequences of this type of failure, we examine the void probability profiles and the film images of Fig. 5b and 5c, respectively. Fig. 5b shows that while voids can appear anywhere in the film, they show a modestly higher tendency for forming near the neutral substrates. The film configurations of Fig. 5c confirm that the strain-induced voids that form in the thicker film are also "bubble-like" like in Fig. 4c, as opposed to the planar voids observed in the ultrathin films of Fig. 2 and 3.

Finally, we point out there is an additional structural consequence of transverse cohesive failure. Since the initiating voids have a modest preference for forming near substrates with weak attractions, and since they grow in size upon the application of strain, they can ultimately lead to a secondary adhesive failure event. This simply means that it may not be easy to distinguish between adhesive and transverse cohesive modes of failure "after the fact", i.e., by only examining the final structure of the failed sample. In contrast, we do not find a similar strain-induced cascading of failure events for thin films confined between strongly attractive substrates.

4   Summary and Conclusions

To complete our nanoscale film analysis, the main features of the EOSELs for all 9 films studied are summarized in Table 1. The information provided includes the film thickness L, the well-depth of the film-substrate potential ϵ_w/ϵ_{fw}, the direction ($\parallel$ or $\perp$) of vulnerability to mechanical failure (i.e., which stress component shows a maximum at a higher density), and the corresponding density where this occurs ρ_S (i.e., the Sastry density (Sastry et al., 1997; Debenedetti et al., 1999) for the film).

The main trends make good physical sense. For thicker films, we see a crossover in vulnerabilities from normal cohesive failure (when confined between strongly attractive substrates) to transverse cohesive failure (when confined between weakly attractive substrates). In the former case, strong bonding to the substrates tears the film apart upon the application of strain, whereas the film ruptures under its own strain-induced cohesive forces if the substrates are only weakly attractive. These purely energetic trends are in qualititative agreement with the predictions of a recently introduced energy landscape-based theory for films (Mittal et al., 2004; Truskett and Ganesan, 2003). In the thicker film cases discussed above, the weak spots where voids form appear "bubble-like", similar to bulk material behavior. For ultrathin films, we find a crossover in vulnerabilities from cohesive failure (when confined between strongly attractive substrates) to adhesive failure (when confined between weakly attractive substrates). Films that fail cohesively have much higher tensile strength and toughness. These trends are in line with those seen in recent MD simulations of dynamic failure in polymer thin-film adhesives (Gersappe and Robbins, 1999). In the ultrathin film cases, the weak spots appear planar (parallel to the sub-

strates), and their location is strongly influenced by the inhomogeneous structural layering of the films.

In spite of the intriguing results provided by the present analysis of the EOSELs for model thin films, there are many open issues that warrant future study. Even if we confine ourselves to EOSEL thin-film studies, there remains a need to understand how factors such as substrate morphology and/or the effects of "free" interfaces impact material stability. Neither of these issues are addressed in the present work. The question of how molecular connectivity and architecture (from small molecules to polymers) can impact the mechanical strength, structure, and the possible mechanisms for failure is also of great fundamental and practical importance. For instance, would molecules of ellipsoidal shape show fundamentally different behavior from the spherically-symmetric molecules studied here, since the former have been shown (Donev et al., 2004) to pack much more efficiently than the latter (Torquato et al., 2000; Truskett et al., 2000)? Furthermore, how does the present picture change if one considers the EOSEL under plane stress rather than plane strain conditions? What about failure occuring under shear deformations? Finally, the role that failure mechanisms obtained via quasistatic analyses play in actual dynamic failure processes is still far from resolved, and it is a issue that demands further scrutiny.

Acknowledgements

It is a pleasure to present this work about mechanical properties, structural inhomogeneities, and void-space geometry in nanoscale films for an issue honoring Salvatore Torquato. He is a lifelong mentor to one of us (TMT) and has contributed greatly to the current state of knowledge on these fascinating

References

Born, M., Huang, K., 1954. Dynamical Theory of Crystal Lattices, Claredon Press, Oxford.

Capaldi, F. M., Boyce, M. C., Rutledge, G. C., 2002. Enhanced mobility accompanies the active deformation of a glassy amorphous polymer. Phys. Rev. Lett. 89, 175505[1-4].

Debenedetti, P. G., Stillinger, F. H., Truskett, T. M., Roberts, C. J., 1999. The equation of state of an energy landscape. J. Phys. Chem. B 103, 7390-7397.

Debenedetti, P. G., Truskett, T. M., Lewis, C. P., Stillinger, F. H., 2001. Theory of supercooled liquids and glasses: Energy landscape and statistical geometry perspectives. Adv. Chem. Eng. 28, 21-79.

Donev, A., Cisse, I., Sachs, D., Variano, A. Stillinger, F. H. Connelly, R., Torquato, S. and Chaikin, P. M., 2004. Improving the density of jammed disordered packings using elipsoids. Science 303, 990-993.

Ebner, C., Saam, W. F., 1977. New phase-transition phenomena in thin argon films. Phys. Rev. Lett. 38, 1486-1489.

Falk, M. L., Langer, J. S., 1998. Dynamics of viscoplastic deformation in amorphous solids. Phys. Rev. E 57, 7192-7205.

Forrest, J. A., Dalnoki-Veress, K., 2001. The glass transition in thin polymer films. Adv. Colloid Interface Sci. 94, 167-195.

Gelb, L. D., Gubbins, K. E., Radhakrishnan, R., Sliwinska-Bartkowiak, M., 1999. Phase separation in confined systems. Rep. Prog. Phys. 62, 1573-1659.

Gersappe, D., Robbins, M. O., 1999. Where do polymer adhesives fail?. Europhys. Lett. 48, 150-155.

Gersappe, D., 2002. Molecular mechanisms of failure in polymer nanocomposites. Phys. Rev. Lett. 89, 058301[1-4].

Hutchinson, J. W., Suo, Z., 1992. Mixed mode cracking in layered materials, in: Hutchinson, J. W., Wu, T. Y. (Eds.), Advances in Applied Mechanics. Academic Press, San Diego, pp. 63-191.

Hutnik, M., Argon, A. S., Suter, U. W., 1993. Simulation of elastic and plastic response in the glassy polycarbonate of 4,4-isopropylidenediphenol. Macromolecules 26, 1097-108.

Irving, J. H., Kirkwood, J. G., 1950. The statistical mechanical theory of transport processes. IV. The equation of hydrodynamics. J. Chem. Phys. 18, 817-829.

Liu, D. C., Nocedal, J., 1989. On the limited memory method for large scale optimization. Math. Program. B 45, 503-528.

Lund, A. C., Schuh, C. A., 2003a. Yield surface of a simulated metallic glass. Acta Mater. 51, 5399-5411.

Lund, A. C., Schuh, C. A., 2003b. Driven alloys in the athermal limit. Phys. Rev. Lett. 91, 235505[1-4].

Malandro, D. L., Lacks, D. J., 1997. Volume dependence of potential energy landscapes in glasses. J. Chem. Phys. 107, 5804-5810.

Malandro, D. L., Lacks, D. J., 1998. Molecular-level mechanical instabilities and enhanced self-diffusion in flowing liquids. Phys. Rev. Lett. 81, 5576-5579.

Malandro, D. L., Lacks, D. J., 1999. Relationships of shear-induced changes in the potential energy landscape to the mechanical properties of ductile glasses. J. Chem. Phys. 110, 4593-4601.

Maloney C., Lemaître, A., 2004a. Subextensive scaling in the athermal, quasistatic limit of amorphous matter in plastic shear flow. Phys. Rev. Lett. 93, 016001[1-4].

Maloney C., Lemaître, A., 2004b. Universal breakdown of elasticity at the onset of material failure. Phys. Rev. Lett. 93, 195501[1-4].

Mittal, J., Shah, P., Truskett, T. M., 2004. Using energy landscapes to predict the properties of thin films. J. Phys. Chem. B, 108, 19769-19779.

Mott, P. H., Argon, A. S., Suter, U. W., 1993. Atomistic modelling of plastic deformation of glassy polymers. Phil. Mag. A 67, 931-978.

Roberts, C. J., Debenedetti, P. G., Stillinger, F. H., 1999. Equation of state of the energy landscape of SPC/E water. J. Phys. Chem. B 46, 10258-10265.

Rottler, J., Robbins, M. O., 2001. Yield conditions for deformation of amorphous polymer glasses. Phys. Rev. E 64, 051801[1-8].

Rottler, J., Robbins, M. O., 2003. Shear yielding of amorphous glassy solids: Effect of temperature and strain rate. Phys. Rev. E 68, 011507[1-10].

Sastry, S., Debenedetti, P. G., Stillinger, F. H., 1997. Statistical geometry of particle packings. II. "Weak spots" in liquids. Phys. Rev. E 56, 5533-5543.

Shen, V. K., Debenedetti, P. G., Stillinger, F. H., 2002. Energy landscape and isotropic tensile strength of n-alkane glasses. J. Phys. Chem. B 106, 10447-10459.

Stevens, M. J., 2001. Interfacial fracture between highly cross-linked polymer networks and a solid surface: Effect of interfacial bond density. Macromolecules 34, 2710-2718.

Stillinger, F. H., Weber, T. A., 1982. Hidden structures in liquids. Phys. Rev. A 25, 978-989.

Torquato, S., Truskett, T. M., Debenedetti, P. G., 2000. Is random close pack-

ing of spheres well defined? Phys. Rev. Lett. 84, 2064-2067.

Truskett, T. M., Ganesan, V., 2003. Ideal glass transitions in thin films. J. Chem. Phys. 119, 1897-1900.

Truskett, T. M., Torquato, S., Debenedetti, P. G., 2000. Towards a quantification of disorder in materials: Distinguishing equilibrium and glassy sphere packings. Phys. Rev. E 62, 993-1001.

Utz, M., Debenedetti, P. G., Stillinger, F. H., 2001. Isotropic tensile strength of molecular glasses. J. Chem. Phys. 114, 10049-10057.

Van Workum, K., de Pablo, J. J., 2003. Computer simulation of the mechanical properties of amorphous polymer nanostructures. Nano Lett. 3, 1405-1410.

Varnik, F., Bocquet, L., Barrat, J.-L., 2004. A study of the static yield stress in a binary Lennard-Jones glass. J. Chem. Phys. 120, 2788-2801.

Yoshimoto, K., Jain, T. S., Van Workum, K., Nealey, P. F., de Pablo, J. J., 2004. Mechanical heterogeneities in model polymer glasses at small length scales. Phys. Rev. Lett. 93, 175501[1-4].

Figure Captions

(1) Schematic of the relationship between inherent structure (IS) pressure and density, the so-called equation of state of an energy landscape (EOSEL). (a) In bulk isotropic materials, inherent structures formed at densities above the Sastry density ρ_S are structurally homogeneous. Those formed at densities below ρ_S, the state of maximum isotropic tensile stress, contain voids or fissures (Sastry et al., 1997; Debenedetti et al., 1999). (b) Schematic of the EOSEL for a thin film, showing the diagonal components of the inherent structure pressure tensor in the transverse ($p_{IS}^{\parallel}$) and normal ($p_{IS}^{\perp}$) directions.

(2) (a) EOSEL of an ultrathin film ($L = 5$) confined between weakly attractive substrates ($\epsilon_w = 0.2\epsilon_{fw}$), depicting normal ($\square$) and transverse ($\triangleright$) components of the inherent structure pressure tensor. Also shown is the corresponding probability of finding of voids ($\circ$) in the film. (b) Void probability distribution $P(z)$ in the normal direction for $\rho = 0.2, 0.65, 0.66$, and 1.0. The arrow indicates increasing density (decreasing transverse strain). (c) Visual depiction of inherent structure configurations for densities $\rho = 0.5$ (left) and $\rho = 0.66$ (right). These illustrate where planar voids form near the substrate, indicating an adhesive failure mechanism.

(3) (a) EOSEL of an ultrathin film ($L = 5$) confined between strongly attractive substrates ($\epsilon_w = 5\epsilon_{fw}$), depicting normal ($\square$) and transverse ($\triangleright$) components of the inherent structure pressure tensor. Also shown is the corresponding probability of finding of voids ($\circ$) in the film. (b) Void probability distribution $P(z)$ in the normal direction for $\rho = 0.2, 0.3, 0.76$,

and 1.0. The arrow indicates increasing density (decreasing transverse strain). (c) Visual depiction of inherent structure configurations for densities $\rho = 0.5$ (left) and $\rho = 0.76$ (right). These illustrate where planar voids form in between molecular layers, indicating a cohesive failure mechanism.

(4) (a) EOSEL of a thicker film ($L = 10$) confined between strongly attractive substrates ($\epsilon_w = 5\epsilon_{fw}$), depicting normal ($\square$) and transverse ($\triangleright$) components of the inherent structure pressure tensor. Also shown is the corresponding probability of finding of voids ($\circ$) in the film. (b) Void probability distribution $P(z)$ in the normal direction for $\rho = 0.2, 0.86, 0.87$, and 1.0. The arrow indicates increasing density (decreasing transverse strain). (c) Visual depiction of inherent structure configurations for densities $\rho = 0.6$ (left) and $\rho = 0.82$ (right). These illustrate where "bubble-like" voids form in the film, consistent with a normal cohesive failure mechanism.

(5) (a) EOSEL of a thicker film ($L = 10$) confined between neutral substrates ($\epsilon_w = \epsilon_{fw}$), depicting normal ($\square$) and transverse ($\triangleright$) components of the inherent structure pressure tensor. Also shown is the corresponding probability of finding of voids ($\circ$) in the film. (b) Void probability distribution $P(z)$ in the normal direction for $\rho = 0.2, 0.81, 0.82$, and 1.0. The arrow indicates increasing density (decreasing transverse strain). (c) Visual depiction of inherent structure configurations for densities $\rho = 0.4$ (left) and $\rho = 0.82$ (right). These illustrate where "bubble-like" voids form near the substrates, consistent with a transverse cohesive failure mechanism.
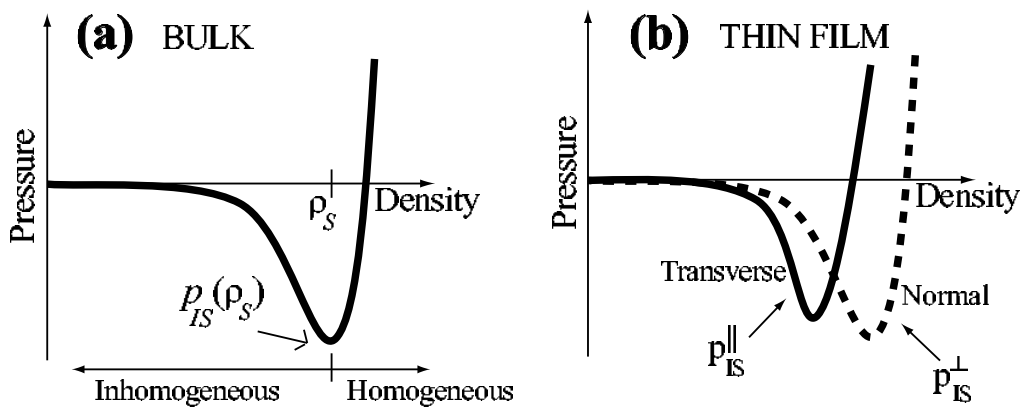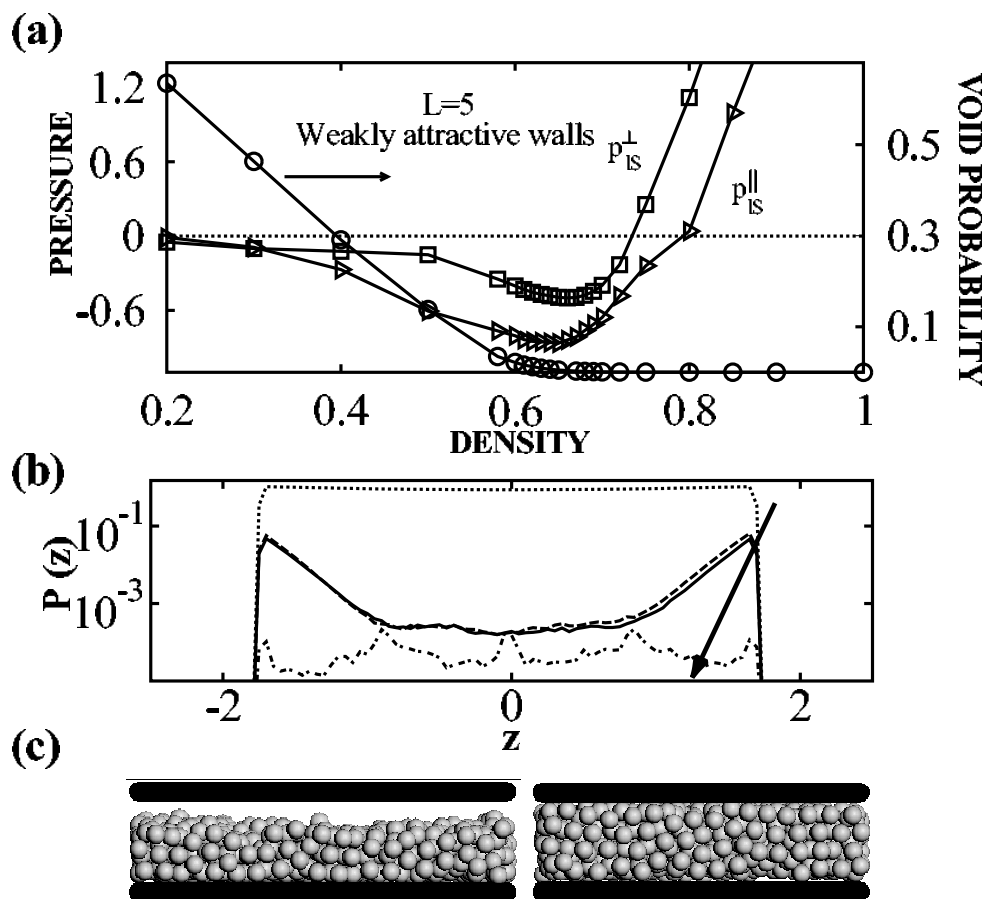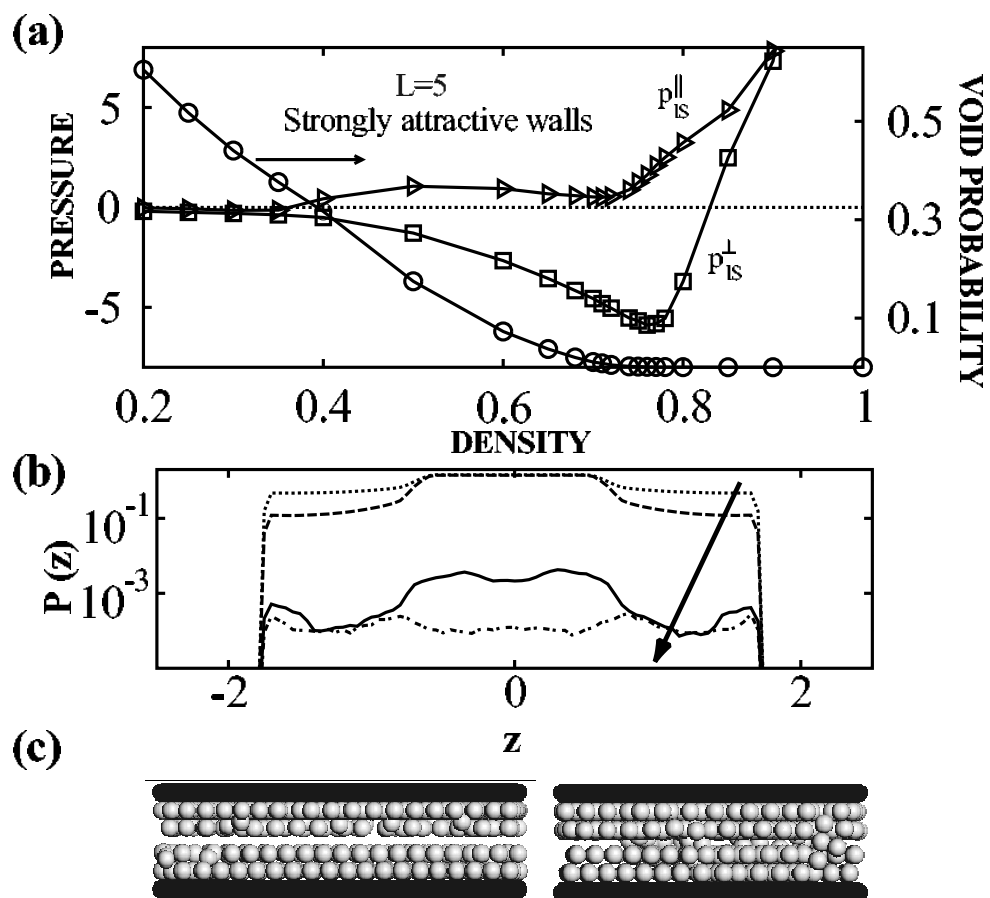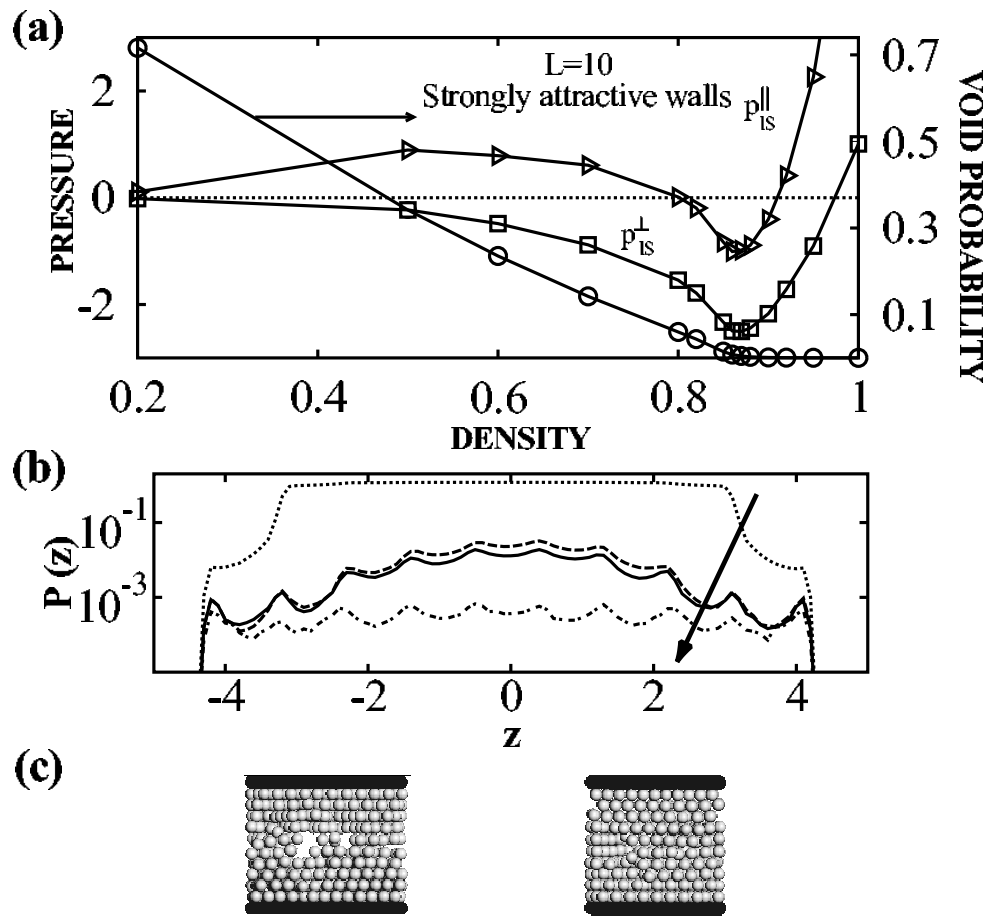
Fig. 1.

Fig. 2.

(a)

PRESSURE

L=5
Strongly attractive walls

$p_{IS}^{\parallel}$

$p_{IS}^{\perp}$

VOID PROBABILITY

DENSITY

(b)

P (z)

z

(c)

Fig. 3.

(a) L=10
Strongly attractive walls $p_{IS}^{\parallel}$

PRESSURE

VOID PROBABILITY

$p_{IS}^{\perp}$

DENSITY

(b)

$P(z)$

z

(c)

Fig. 4.

(a)

L=10
Neutral Walls

PRESSURE

VOID PROBABILITY

$p_{ls}^{\perp}$

$p_{ls}^{\parallel}$

DENSITY

(b)

P (z)

10^{-1}

10^{-3}

z

(c)

Fig. 5.

L	ϵ_w/ϵ_{fw}	Failure direction	ρ_S
	5.0	$\perp$	0.87
10	1.0	$\parallel$	0.82
	0.2	$\parallel$	0.82
	5.0	$\perp$	0.85
7.5	1.0	$\perp$	0.81
	0.2	$\parallel$	0.77
	5.0	$\perp$	0.76
5	1.0	$\perp$	0.70
	0.2	$\perp$	0.66

Table 1

Summary of the main features of the EOSELs for 9 films: film thickness L, the well-depth of the film-substrate potential ϵ_w/ϵ_{fw}, the primary direction ($\parallel$ or $\perp$) of vulnerability to mechanical failure, and the corresponding density where this occurs ρ_S (i.e., the Sastry density for the film).